Received: 25 January 2022 | Revised: 29 March 2022 | Accepted: 6 April 2022

DOI: 10.1002/pro.4319

FULL-LENGTH PAPER

THE PROTEIN SOCIETY WILEY

Structural and functional characterization of TrmM in m^6A modification of bacterial tRNA

Hyeonju Jeong | **Yeji Lee** | **Jungwook Kim**

Department of Chemistry, Gwangju Institute of Science and Technology, Gwangju, Korea

Correspondence
Jungwook Kim, Department of Chemistry, Gwangju Institute of Science and Technology, Gwangju 61005, Korea.
Email: jwkim@gist.ac.kr

Funding information
National Research Foundation of Korea, Grant/Award Number: NRF-2021R1A2C2009773

Review editor: John Kuriyan

Abstract

N^6-methyladenosine (m^6A), widely distributed in both coding and noncoding RNAs, regulates the epigenetic signals and RNA metabolism in eukaryotes. Although this posttranscriptional modification is frequently observed in messenger and ribosomal RNA, it is relatively rare in transfer RNA. In *Escherichia coli*, TrmM encoded by *yfiC* is the tRNA-specific N^6 methyltransferase, which modifies the A37 residue of $tRNA^{Val}$ (cmo^5UAC) using *S*-adenosyl-L-methionine as a methyl donor. However, the structure–function relationship of this enzyme is not completely understood. In this report, we determined two x-ray crystal structures of *Mycoplasma capricolum* TrmM with and without *S*-adenosyl-L-homocysteine, which is a reaction product. We also demonstrated the cellular and in vitro activities of this enzyme in the m^6A modification of tRNA and the requirement of a divalent metal ion for its function, which is unprecedented in other RNA N^6 methyltransferases, including the *E. coli* TrmM. Our results reveal that the dimeric form of *M. capricolum* TrmM is important for efficient tRNA binding and catalysis, thereby offering insights into the distinct substrate specificity of the monomeric *E. coli* homolog.

KEYWORDS

m^6A, methyltransferase, protein crystal, tRNA modification, x-ray structure

1 | INTRODUCTION

Over 150 posttranscriptional modifications are observed in cellular RNAs, most of which are concentrated in tRNAs.[1] The anticodon stem-loop (ASL) is the most heavily modified region of tRNA, especially at the 34th and 37th positions.[1,2] Posttranscriptional modifications of these nucleotides enhance the decoding process, including translation fidelity,[3–5] frameshift,[6–8] translocation,[9,10] ribosome binding,[11,12] and aminoacylation.[13,14] ASL modifications play important roles in the regulation of translation in response to various types of stress.[15–17] The 37th position within tRNA, 3′ adjacent to the third nucleotide of the anticodon, is generally occupied by a purine. To date, more than 10 modifications at the 37th position of tRNA have been reported,[1,2] where N^1-methylguanosine (m^1G), N^2-methyladenosine (m^2A), N^6-methyladenosine (m^6A), N^6-isopentenyladenosine (i^6A), N^6-threonylcarbamoyladenosine (t^6A), and their derivatives were identified in *Escherichia coli* tRNAs (Figure 1a). These nucleobase modifications can potentially affect the base-pairing and local conformation of polynucleotides; for example, m^1G blocks base-pairing and induces local duplex melting in RNA.[18] Analysis of solution structures of ASL containing i^6A37 revealed that the modification disrupts the intraloop hydrogen bond to increase flexibility, which helps stabilize the open conformation of the anticodon loop and forms the characteristic

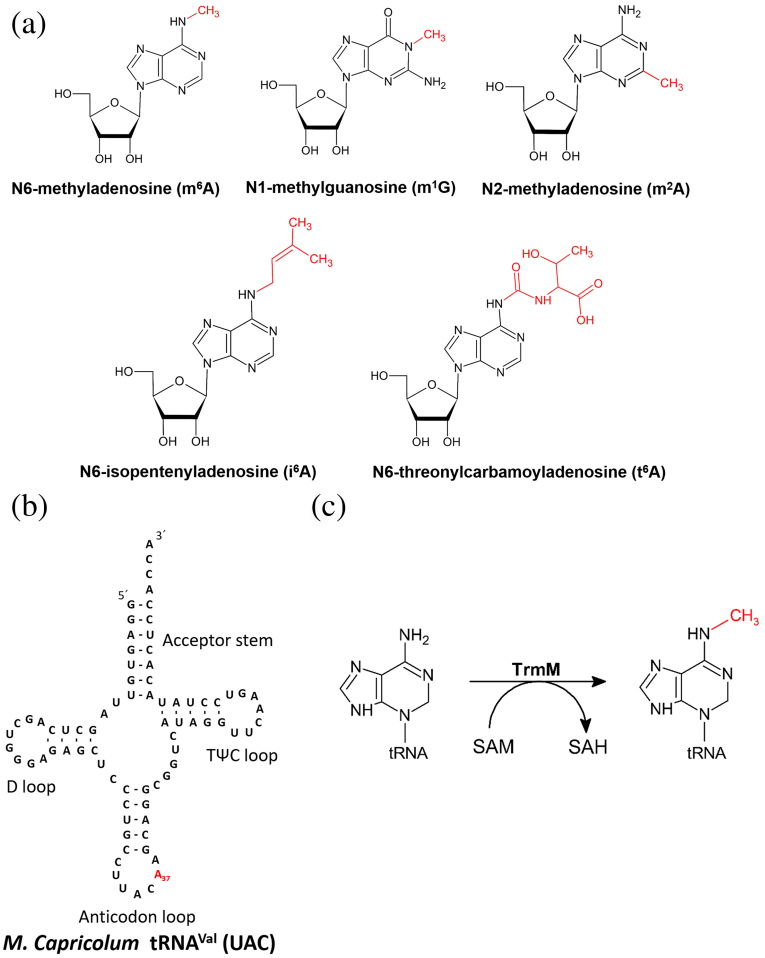

FIGURE 1 tRNA modifications at position 37. (a) Chemical structures of modified nucleosides at the 37th position, where posttranscriptional modifications are highlighted in red. (b) Cloverleaf representation of the secondary structure of *Mycoplasma capricolum* $tRNA^{Val}$ (UAC). (c) Methyl transfer reaction by TrmM involved in m^6A37 modification

U-turn motif.[19–21] In the structure of t^6A37 harboring ASL, the extended planar structure of the modified base enhances the stacking with nearby bases, which stabilizes the codon–anticodon interactions more than the unmodified tRNA.[22,23]

m^6A is relatively rare in tRNA and mostly observed in bacteria. The biosynthetic pathway leading to the m^6A37 modification in tRNA was discovered by Golovina et al., where TrmM in *E. coli* was identified as a tRNA-specific methyltransferase (Uniprot ID: P31825, formerly designated as YfiC or TrmN6), which installs the methyl group on the exocyclic nitrogen (N^6) of A37 residue in $tRNA^{Val}$ (cmo^5UAC).[24] Deletion of *trmM* does not significantly affect the fitness of the mutant strain under normal growth conditions, although this modification is important for enhancing cell survival during osmotic and oxidative stress. However, an experimentally determined structure of TrmM is not currently available. Notably, m^6A37 modification appears to be quite common in *Mollicutes*, such as *Mycoplasma mycoides* and *M. capricolum*, based on the published tRNA sequences; for example, 12 out of 29 tRNAs of *M. capricolum* contain m^6A at the 37th position.[25] However, the enzyme responsible for m^6A37 modification has not yet been verified in these organisms, although a position-specific iterative-basic local alignment search for TrmM in *M. capricolum* returns MCAP_0012, which shares 21.6% sequence identity with the *E. coli* homolog. Previously, MCAP_0012 was predicted to be a tRNA O2'-MTase along with *E. coli* YfiC and *Bacillus subtilis* YabB before the characterization of *E. coli YfiC* as an N^6 MTase.[26]

In this study, we experimentally proved that MCAP_0012 is the TrmM of *M. capricolum* (denoted as Mc_TrmM hereafter), which methylates the N^6 of A37 residue of tRNA using *S*-adenosyl-L-methionine (SAM) as a methyl donor to produce m^6A37 and *S*-adenosyl-L-homocysteine (SAH) (Figure 1b,c). Furthermore, two x-ray crystal structures of Mc_TrmM were determined, with and without SAH, representing the first 3D structure of tRNA-specific N^6 MTase. Using this structural information combined with various biochemical data, we sought to unveil the molecular basis underlying TrmM–tRNA interactions, which can provide fundamental insights into the mechanism of chemical transformation and key determinants of substrate specificity during m^6A modification of tRNA.

2 | RESULTS

2.1 | Mc_TrmM can substitute YfiC in *E. coli*

Mc_TrmM shares 22% sequence identity with *E. coli* YfiC or TrmM (Ec_TrmM), the only tRNA N^6 MTase known to date. To test whether Mc_TrmM could function as a tRNA-specific N^6 methyltransferase in bacterial cells, we performed a gene complementation assay using a *trmM*-deletion mutant (Δ*trmM*) of *E. coli*. Since *E. coli* rRNA also contains m^6A, we carefully extracted the total tRNA from the cellular RNA pool to minimize rRNA contamination, as described in Supplementary Methods S1. Our high-performance liquid chromatography (HPLC) and liquid chromatography-mass spectrometry (LC–MS) data showed that m^6A was not detectable in the total tRNA samples derived from Δ*trmM* cells transformed with an empty plasmid. Meanwhile, the m^6A signal was clearly observed in the tRNA sample when the mutant strain was complemented with a plasmid harboring the *M. capricolum trmM* gene (Figure 2), which strongly suggests that Mc_TrmM is a tRNA N^6 MTase.

2.2 | Mc_TrmM requires a divalent metal ion for activity

To validate whether Mc_TrmM was necessary and sufficient for the N^6 methylation of tRNA, we purified recombinant Mc_TrmM using *E. coli* as the expression host and performed in vitro assays using tRNA substrates prepared from the T7-RNA polymerase reaction (Figure S1). Surprisingly, the installation of the methyl group was detected in our HPLC and LC–MS analyses only when a divalent metal ion was provided in the assay mixture (Figure 3 and Figure S2). We initially tested various metal ions for the methyl transfer assay and found that Mc_TrmM was most active with Mg^{2+}, Mn^{2+}, Ca^{2+}, or Fe^{2+} but inactive with Fe^{3+} or Zn^{2+}. The enzyme displayed a marginal activity with Co^{2+}. In contrast, the metal dependence of Ec_TrmM has not yet been reported.[24] Using inductively coupled plasma mass spectrometry, we examined the metal content of recombinant Mc_TrmM samples, which were incubated with 5 mM divalent metal ions, followed by dialysis against a metal-free buffer. However, none of these metal ions were detected in the dialyzed protein sample at a significant level (Table S1), suggesting that the intrinsic metal affinity of the enzyme is very weak and that additional factors may be required for efficient metal binding. Although the identity of the metal required for TrmM cellular activity is currently unknown, Mg^{2+} was chosen as the metal cofactor for our assays.

2.3 | Scope of tRNA substrates for Mc_TrmM

Although only $tRNA^{Val}$ (cmo^5UAC) contains the m^6A37 modification in *E. coli*, 12 tRNA species show this modification in *M. capricolum*. We performed in vitro assays to

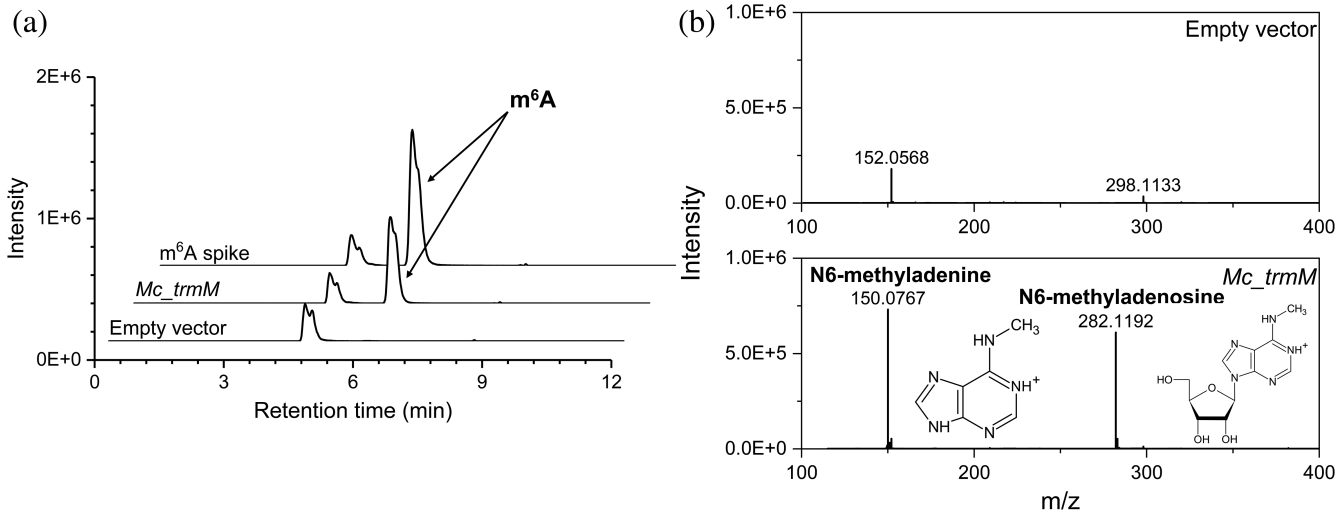

FIGURE 2 Cellular activities of the TrmM of *M. capricolum*. (a) Representative extracted-ion chromatogram of N^6-methyladenosine (m^6A) modification in LC–MS-based analyses of hydrolyzed cellular tRNA. The m^6A formation was rescued in Δ*trmM* cells complemented with the *Mc_trmM*-harboring plasmid but not with an empty vector. (b) Mass spectrum obtained from electrospray ionization (ESI)-quadrupole time-of-flight tandem (QTOF)-MS analysis of the peak shown in (a). The *m/z* values of two major peaks shown are consistent with those of m^6A ($[C_{11}H_{16}N_5O_4]^+ = 282.1202$) and N^6-adenine ($[C_6H_8N_5]^+ = 150.0780$)

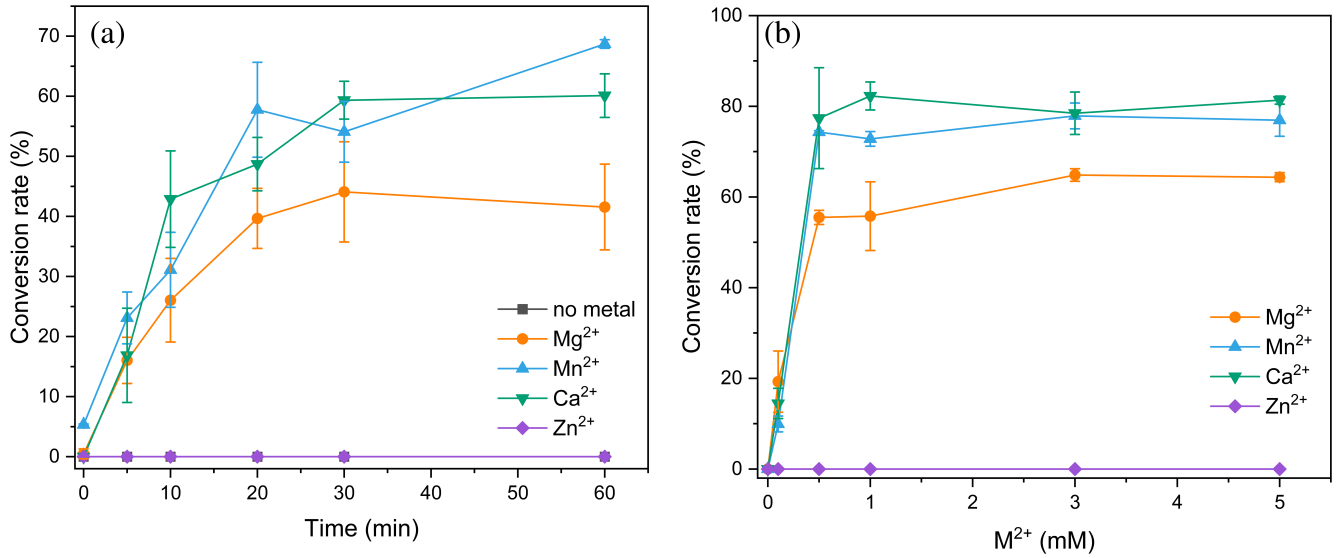

FIGURE 3 Metal-dependent in vitro activity of Mc_TrmM. (a) Time-course measurement of m^6A formation in $tRNA^{Val}$ with or without a divalent metal ion. (b) Formation of m^6A in $tRNA^{Val}$ with varying concentrations of divalent metal ions. Error bars represent the standard deviation of three data sets

determine whether recombinant Mc_TrmM could modify $tRNA^{Val}$, $tRNA^{Leu}$, and $tRNA^{Gln}$. The assay results revealed that Mc_TrmM was capable of installing the methyl group on all three tRNAs, although $tRNA^{Val}$ appeared to be modified more efficiently than the other two (Figure 4a). When the time-course of TrmM-dependent m^6A formation was examined, Mc_TrmM and Ec_TrmM exhibited comparable specific activities in methylating Mc_$tRNA^{Val}$ (Figure 4b). ASL alone appeared to be a poor substrate for Mc_TrmM, and m^6A formation was not detected in our assay when ASL^{Val} was employed as the methyl acceptor. In contrast, Ec_TrmM was able to modify ASL^{Val}, albeit at a much slower rate compared to the full-length version. As expected, Mc_TrmM was able to modify *E. coli* $tRNA^{Val}$ in vitro, complying with the complementation assay results. Notably, the enzyme exhibited substantially higher activity when *M. capricolum* $tRNA^{Val}$, a substrate with a native sequence, was used in the assay.

2.4 | Overall conformation of Mc_TrmM

We determined the x-ray crystal structures of apo and SAH-bound Mc_TrmM, which were built using diffraction data up to 2.16 and 2.52 Å, respectively (Table 1). All protomers in both apo and SAH-bound structures assume a similar conformation, with an rmsd value of C_αs ranging from 0.35 to 0.56 Å. Each monomer adopts a Rossmann-fold, which contains an extended β-sheet composed of seven strands in the core flanked by two strands (β1 and β2) and a helix (α8) in the N- and C-termini, respectively (Figure 5a). The core βαβ-fold conserved in TrmM is a canonical structural attribute of Class I SAM-dependent MTases.[27] The search for structural homologs using SAH-bound structure as a query on the DALI server[28] returned a putative methyltransferase from *Listeria monocytogenes* as a top hit with an rmsd value of 1.3 Å and *z*-score of 31.3 (PDB code 3lpm), which is linked to no publication record.

The SAH-bound structure of Mc_TrmM exhibited a total of four protomers in the asymmetric unit (ASU), which were formed from two weakly associated dimers via a noncrystallographic dyad, whereas a monomer was found in the ASU of the apo-structure (Figure 5b). However, an essentially identical dimer can be reconstituted with a symmetry-related molecule, similar to that observed in the SAH-bound structure. To establish the oligomeric state of the enzyme, we performed multiangle light scattering combined with size exclusion chromatography (SEC-MALS) on recombinantly purified Mc_TrmM and analyzed the data. In line with the crystallographic results, the enzyme appeared to exist as a homodimer in the solution (Figure 5c). Alternatively, Ec_TrmM was shown to be a monomer, as confirmed via SEC experiments (Figure S3). Protein interface analysis using the PISA program[29] also supports the notion that the biological assembly of Mc_TrmM is a dimer, as represented by our structures. The dimer interface was mainly maintained by multiple hydrogen bonds and hydrophobic contact between residues located on α7, loop 8, and loop 9 in both monomers, where no salt bridge could be detected (Figure 5d).

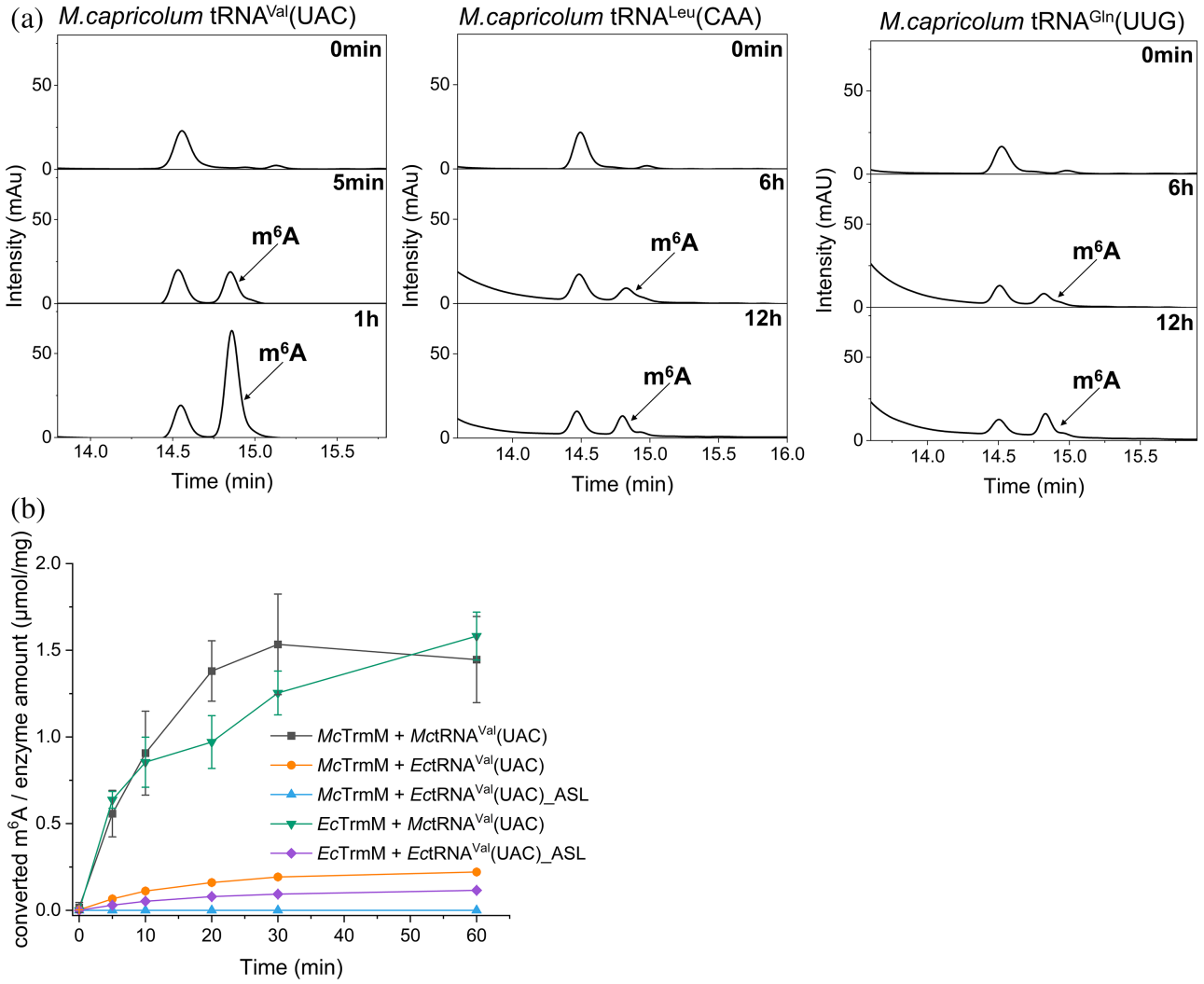

FIGURE 4 Comparison of substrate specificity. (a) HPLC chromatograms showing the time-dependent formation of m^6A by Mc_TrmM with *M. capricolum* $tRNA^{Val}$ (UAC), *M. capricolum* $tRNA^{Leu}$ (CAA), and *M. capricolum* $tRNA^{Gln}$ (UUG). (b) Time-course measurement of specific activities of Mc_TrmM and Ec_TrmM with *M. capricolum* $tRNA^{Val}$ (UAC), *E. coli* $tRNA^{Val}$ (UAC), and *E. coli* $tRNA^{Val}$ (UAC) anticodon stem-loop. Error bars represent the standard deviation of three data sets

Although our in vitro assays revealed the requirement for a divalent metal ion in the methyl transfer reaction, we could not identify the metal-binding site in either of the protein structures. Unfortunately, our attempts to introduce a metal ion into the active site of the protein crystals by increasing the metal concentration during co-crystallization or soaking in combination with the use of different types of divalent metal ions was unsuccessful.

2.5 | Conformational changes induced by cofactor binding

Our SAH-bound structure of Mc_TrmM clearly identified protein-bound cofactors in three of the four protomers (A, C, and D). The overall binding mode of each cofactor is quite similar to one another, featuring an extensive hydrogen-bonding network, as described in Figure 6a,b. In the apo structure, C_α of Asn-50 moves toward Ser-28 by approximately 4.1 Å relative to that in the SAH-bound state and fills in the space, which would have been occupied by the homocysteine moiety (Figure 6c). The largest structural deviation between the apo and SAH-bound structures occurred in the region encompassing loop 6 and a short helix α5 (Phe-119 to Glu-141), which were entirely disordered in the apo structure (Figure 6d). In comparison, the SAH-bound structure exhibited a smaller degree of disorder, which could be modeled completely in protomer A and with a smaller gap in protomers C and D, where residues from Met-122 to Glu-130 are missing. Interestingly, similar to the apo structure, a substantial disorder occurred around loop 6-α5 in protomer B, the only subunit not

TABLE 1 Crystallographic statistics

	Apo	SAH-bound
Data collection		
Wavelength (Å)	1.0000	0.97942
Space group	H 3 2	P 2_1
Cell dimensions		
a, *b*, *c* (Å)	112.71112.71110.18	74.39 75.89 95.54
α, *β*, *γ* (°)	90 90,120	90 95.18 90
Resolution (Å)	30.00–2.15 (2.19–2.15)	47.64–2.54 (2.65–2.54)
R_{merge}	0.082 (0.567)	0.215 (2.385)
$CC_{1/2}$	0.994 (0.898)	0.992 (0.413)
I/σI	5.8 (2.5)	6.9 (1.4)
Completeness (%)	93.3 (91.8)	97.5 (96.9)
Redundancy	5.1 (3.8)	6.2 (6.0)
Refinement		
Resolution (Å)	26.51–2.15	47.64–2.54
No. of unique reflections	13,868	34,125
R_{work}/R_{free}	0.202/0.258	0.209/0.266
No. atoms		
Protein	1,671	6,929
Ligand	0	88
Water	30	31
B-factors		
Protein	49.28	54.56
Ligand	—	54.71
Water	45.77	39.71
R.m.s. deviations		
Bond lengths (Å)	0.008	0.008
Bond angles (°)	0.889	1.024
Ramachandran analysis		
Favored (%)	97.1	94.8
Allowed (%)	2.9	5.2
Outliers (%)	0	0

Note: Dataset was collected from a single crystal. Values in parentheses.

complexed with the cofactor in the SAH-bound structure. Moreover, the N-terminal 25 amino acid residues in protomer B are nontraceable, unlike the other subunits. These N-terminal residues, which comprise β1, β2, and loop 1, exhibit the second-largest conformational difference between the apo and cofactor-bound structures. Although the amino acid residues of the N-terminal and loop6-α5 regions do not directly contact SAH, the binding of the cofactor appears to influence the local conformation around these moieties.

2.6 | Putative tRNA-binding site on Mc_TrmM

The concave shape of the protein conformation around the SAH-binding site appears to be ideal for tRNA docking. A large portion of the putative tRNA-binding pocket is composed of a "substrate-binding loop," which plays a critical role in recognizing RNA substrates in other N^6-methyltransferases.[30–33] Our structural data suggest that loop 6 corresponds to the substrate-binding loop (Phe-119 through Ser-132), which is mostly disordered in both the apo and SAH-bound structures of Mc_TrmM, as described earlier. An entire substrate-binding loop can be traced in protomer A of the SAH-bound structure, where the organization of the loop is augmented by a small contact made by a nearby symmetry-related protomer C′ (Figure S4).

To elucidate the detailed interaction map between tRNA and the protein, we first analyzed the distribution of electrostatic potential in the structure of dimeric Mc_TrmM (Figure 7a). Putative tRNA-binding residues that might have attractive Coulombic interactions with the negatively charged phosphate backbone of an oligonucleotide were identified in two regions, one in each protomer (Figure 7b). Region 1 is defined by a protein surface surrounding the cofactor-binding site, which includes Lys-121, Lys-127, Lys-129, Arg-139, His-140, His-167, Arg-168, and Arg-171. These candidate residues were subjected to alanine mutation and the single mutant proteins were tested for in vitro methyl transfer activity. Notably, R139A and R168A were essentially inactive, whereas the catalytic activities of K121A, K127A, H140A, H167A, and R171A were approximately 10%–50% of those of the wild type (Figure 7c). The second tRNA-contacting region, Region 2, is located in the other protomer of the homodimer, where the distribution of positive charges in Region 2 appears to be contiguous with that of Region 1. Six lysine residues in Region 2 were grouped into two, K40A/K41A/K42A/K43A and K158A/K160A, as multiple alanine mutants were generated. Both mutants showed a severe loss of activity, where no significant activity of the quadruple mutant was detected, and the double mutant exhibited less than 10% activity of the wild type. To verify that the structural integrity of each mutant protein was not seriously compromised as a result of the mutation, each mutant protein was analyzed using SEC (Figure S5). The elution profiles of all tested proteins were similar to that of the wild type, and none of these proteins exhibited aggregate formation, confirming that the reduced activity of the mutant enzymes was not caused by the overall misfolding of proteins.

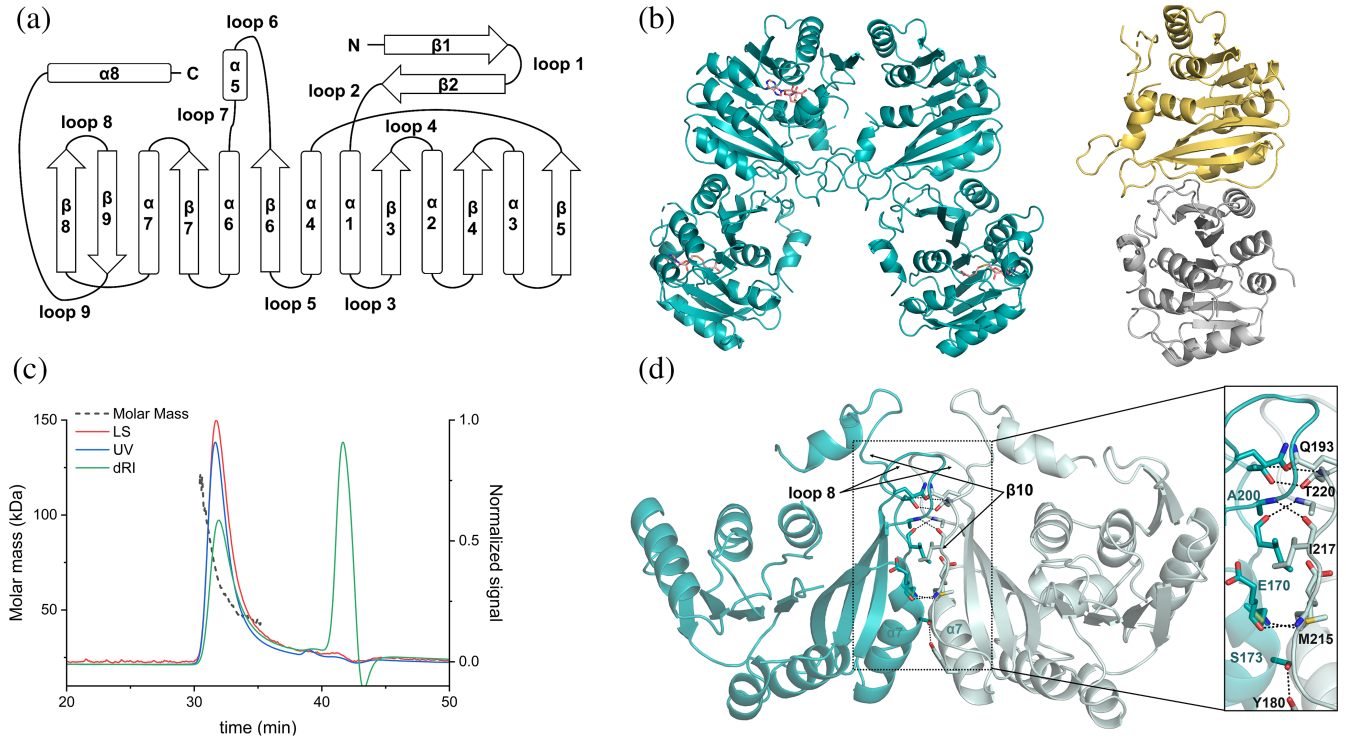

FIGURE 5 Overall structure of Mc_TrmM. (a) Topology diagram based on the S-adenosyl-L-homocysteine (SAH)-bound structure of Mc_TrmM. (b) Contents of the asymmetric units of SAH-bound (cyan) and unbound (yellow) structures of Mc_TrmM are shown on the left and right panels, respectively. The structure of Mc_TrmM complexed with SAH (pink sticks) contains four protomers, whereas the apo structure contains only one. The monomer shown in grey represents a symmetry-related molecule in the crystal of apo protein. (c) Multiangle light scattering combined with size exclusion chromatography (SEC-MALS) result of Mc_TrmM measured using light scattering (red), UV radation (blue), and refractive index (green). Molecular weight is labeled in black (61.35 kDa), which corresponds to the size of the dimer (calculated mass = 57.46 kDa). (d) Dimer interface of TrmM is shown, where the inset illustrates a close-up of molecular interactions between amino acid residues on loop 8, loop 9, and helix 7 from both subunits

3 | DISCUSSION

3.1 | Structure-guided reaction mechanism of Mc_TrmM

Catalytic asparagine or aspartate residue in the highly conserved N/D-PP-Y/F/W (NPPY hereafter) motif in N^6 RNA MTases plays important roles in several aspects of the enzymatic reaction, including participation in SAM binding, enhancement of the nucleophilicity of N^6, and stabilization of a positively charged reaction intermediate.[31,33–36] Structural alignment with the active site residues of the human methyltransferase-like 16 (METTL16): RNA complex implies that a similar strategy for the recognition and methylation of the adenine base may be retained for Mc_TrmM (Figure 8a). The side chain of Asn-116 is estimated to be 3.3 Å away from the nucleophilic adenine N^6 based on the superimposed model. To verify the proposed role of Asn-116, we prepared two mutant proteins of Mc_TrmM, N116D, and N116A and examined their activities via methyl transfer assays. The catalytic activity was completely abolished for both mutant enzymes (Figure 8b), which was surprising as we initially expected N116D to act similar to the wild-type enzyme. Because the side chain of Asn-116 is within a hydrogen-bonding distance from the carboxyl group of SAH, as described in Section 2, we confer that N116D may be inactive owing to the repulsive ionic interactions between the negatively charged side chains of Asp-116 and the carboxyl group of SAM, thus decreasing the binding affinity for the methyl donor.

Based on our collective data, we propose a catalytic mechanism underlying N^6 methylation of A37 by Mc_TrmM, as shown in Figure 8c. In this scheme, Asn-116 participates in the binding of SAM and A37 residue of tRNA. Asn-116 and Pro-117 serve as hydrogen bond acceptors from exocyclic N^6 to enhance nucleophilicity. Furthermore, these hydrogen bonds can stabilize the positively charged methylammonium intermediate formed immediately after methyl transfer. Finally, deprotonation of the methylammonium group completes the m^6A37 modification, presumably in a nonenzymatic manner,

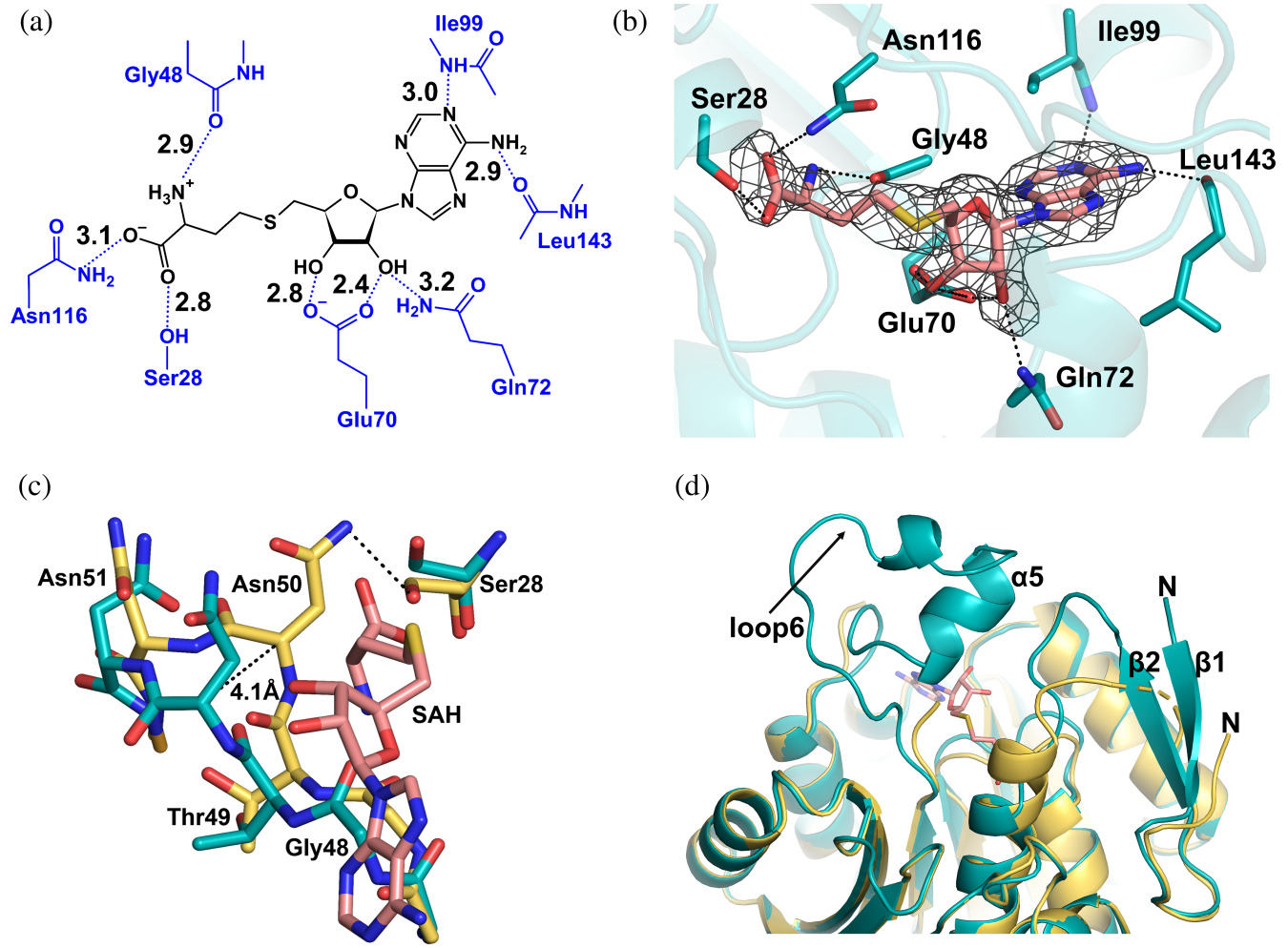

FIGURE 6 Structural changes induced by the binding of SAH. (a) Illustration of the hydrogen-bond network between SAH and Mc_TrmM. The average distance of the hydrogen bond is labeled in Å. (b) Fourier difference map (*Fo* − *Fc*) was calculated without modeling SAH during refinement and displayed as grey mesh contoured at 3.0 sigma. (c) Superimposed active sites showing the local conformational change between the SAH-bound (cyan) and apo (yellow) structures. (d) Superimposition of apo and SAH-bound structures highlighting the locations where the largest conformational deviations are observed. SAH is shown as pink sticks

considering the strong acidity of the intermediate.[37] The aromatic side chain of Tyr-119 aids in the proper positioning of the target adenine base for efficient nucleophilic attack on SAM via critical π-stacking interactions. However, we do not currently understand the exact role of divalent metal ions during catalysis, despite our kinetic data indicating that they are essential for catalytic activity. The requirement of metal ions has not yet been reported for other RNA N^6 MTases. Meanwhile, the bacterial tRNA m^1G37 MTase, TrmD, is dependent on the divalent metal ion, Mg^{2+}.[38,39] The primary role of the ion is proposed to be optimizing the active site geometry and the conformation of SAM based on a molecular dynamics simulation and quantum mechanics study.[39] For Mc_TrmM, metal binding may involve additional components, such as tRNA. Metals bound to tRNA sometimes contribute to the correct conformation or folding of polynucleotides. There is an alternative possibility that both enzymes and tRNA participate in coordinating metal ions and increasing their affinities in a synergistic manner. Once bound, the metal may influence the rearrangement of tRNA and/or protein conformation that is necessary for methyl transfer to occur. The metal cofactor likely dissociates instantly after methylated tRNA is released from the enzyme. A high-resolution structure of the protein–tRNA complex will be valuable in examining this hypothesis and revealing the functional role of the metal.

3.2 | A model for the TrmM–tRNA complex

Structure-guided mutagenesis of potential tRNA-binding residues combined with kinetic analysis supports the idea

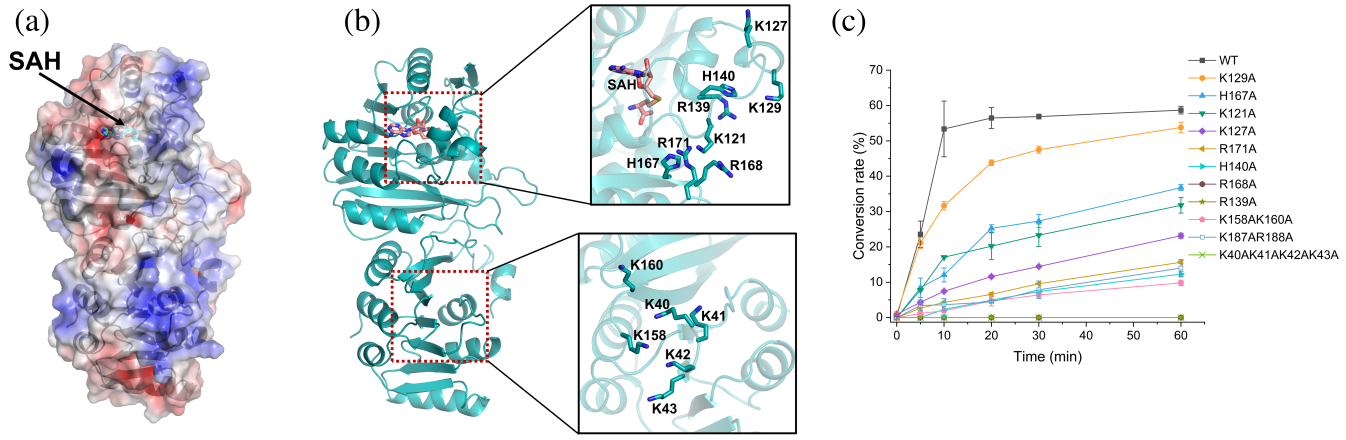

FIGURE 7 Putative tRNA-binding site. (a) Electrostatic potential mapped on the surface of dimeric Mc_TrmM, where positive charges are shown in blue, negative charges in red, and neutral charges in white. SAH is represented by light-blue sticks. (b) Distribution of basic residues targeted for mutagenesis, which were grouped into Region 1 (top inset) and Region 2 (bottom inset), are highlighted. (c) In vitro enzymatic activities of the wild-type and alanine mutants of basic residues. Notably, the curves from R139A and R168A are overlapped with that of K40A/K41A/K42A/K43A, where they did not exhibit any detectable activity. Error bars represent the standard deviation of three data sets

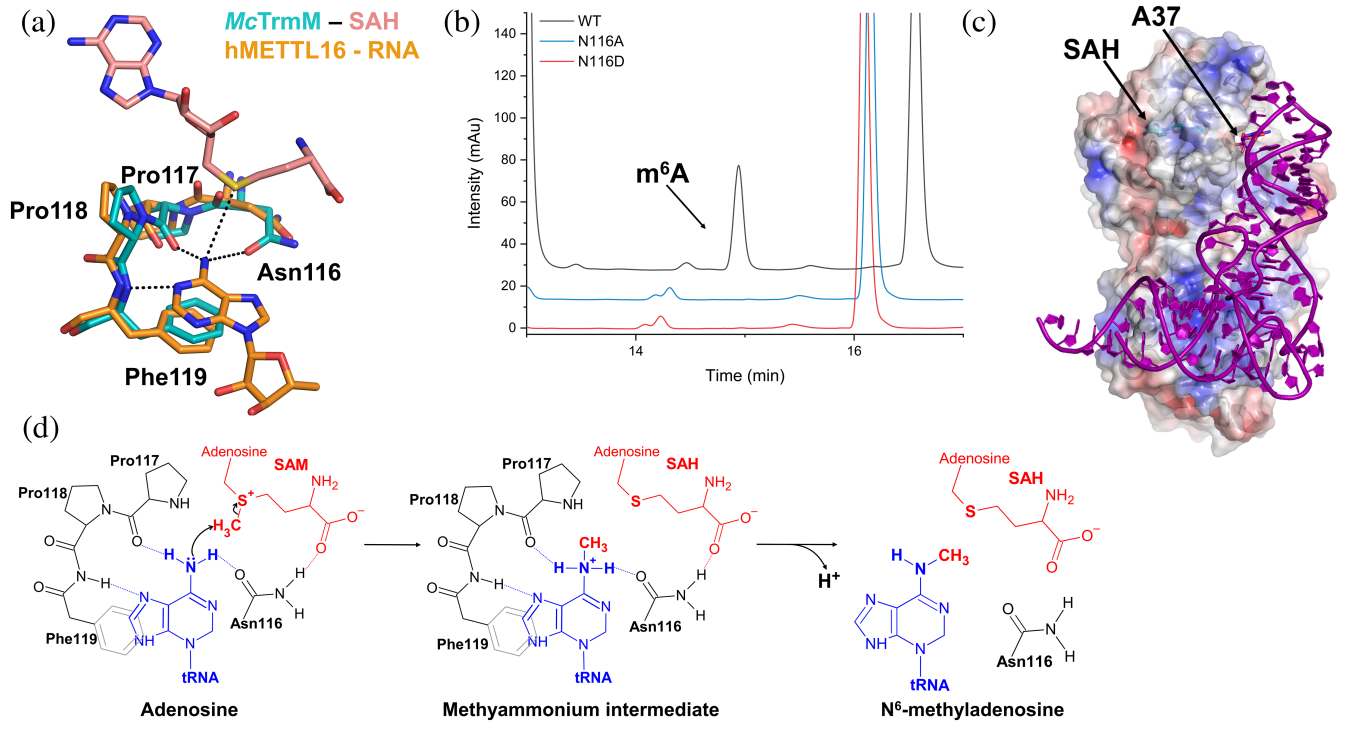

FIGURE 8 Proposed reaction mechanism of Mc_TrmM. (a) Close-up of the superimposed active sites of SAH-bound Mc_TrmM (cyan) with the methyltransferase-like 16 (METTL16)–RNA complex (orange). (b) Comparison of the in vitro activities of the wild-type, N116A, and N116D mutants of Mc_TrmM. (c) Proposed reaction mechanism of Mc_TrmM underlying m^6A37 tRNA modification. (d) Docking model of Mc_TrmM-*E. coli* $tRNA^{Val}$(UAC) complex

that selective basic amino acid residues spread over both protomers may serve as docking platforms for tRNA. As shown in Figure S4, all the mutant proteins tested were stable after purification and appeared to exist in a globular conformation, as opposed to forming an aggregate. However, we cannot rule out the possibility that the decreased activity exhibited by several mutant proteins may have originated from critical events other than defective tRNA binding. We constructed an in silico model of the Mc_TrmM-tRNA–SAH complex from SAH-bound Mc_TrmM and *E. coli* $tRNA^{Val}$ (PDB code 7EQJ[40]) structures using the HDOCK server,[41] which revealed

some interesting points that are consistent with our experimental results (Figure 8d). First, most of the basic residues in Regions 1 and 2 participate in making contact with nearly the entire tRNA molecule, which explains why ASL alone is not a good substrate for the enzyme. Second, extensive interaction with tRNA requires the dimeric form of the enzyme, which is distinct from monomeric Ec_TrmM. The difference in substrate specificity between the two homologs is likely related to dissimilar strategies for binding and recognizing tRNA. Lastly, loops 6 and 8, along with the N-terminal region, contribute to the formation of the tRNA-binding pocket, which appears to accommodate the ASL domain. These moieties, in particular, were shown to be the most flexible parts of the enzyme based on our structures and are expected to undergo large conformational changes upon tRNA binding as well as reorganization of the anticodon loop accompanying the base-flipping of A37, as observed in other cases.[42–45]

In summary, we have verified the cellular and biochemical activities of Mc_TrmM in the N^6-methylation of A37 residue in bacterial tRNA. Furthermore, two x-ray crystal structures of the enzyme, complexed with and without SAH, were determined. This novel structural information on Mc_TrmM can improve our understanding of the key enzymatic features, such as molecular determinants for substrate specificity and reaction mechanisms, of tRNA N^6 MTases. With distantly related Ec_TrmM, these two homologs constitute another interesting example of divergently evolved enzymes in bacterial tRNA modification.

4 | MATERIALS AND METHODS

Detailed description of experimental procedures is included in Supplementary Material S1.

ACKNOWLEDGMENT

This research was supported by Basic Science Research Program through the National Research Foundation of Korea (NRF) (grant number: NRF-2021R1A2C2009773). The authors thank the scientists at beamlines 5C and 11C in Pohang Accelerator Laboratory for support with the x-ray diffraction data collection.

AUTHOR CONTRIBUTIONS

Hyeonju Jeong: Data curation (lead); formal analysis (lead); investigation (lead); visualization (lead); writing – original draft (supporting); writing – review and editing (supporting). **Yeji Lee:** Data curation (supporting); investigation (supporting). **Jungwook Kim:** Conceptualization (lead); formal analysis (lead); funding acquisition (lead); resources (lead); supervision (lead); writing – original draft (lead); writing – review and editing (lead).

DATA AVAILABILITY STATEMENT

Atomic coordinates and structure factors related to this work have been deposited in the PDB with accession numbers 7WM5 and 7WM6

ORCID

Jungwook Kim https://orcid.org/0000-0001-5213-9299

REFERENCES

1. Boccaletto P, MacHnicka MA, Purta E, et al. MODOMICS: A database of RNA modification pathways. 2017 update. Nucleic Acids Res. 2018;46:D303–D307.
2. Juhling F, Morl M, Hartmann RK, Sprinzl M, Stadler PF, Putz J. tRNAdb 2009: Compilation of tRNA sequences and tRNA genes. Nucleic Acids Res. 2009;37:D159–D162.
3. Joshi K, Bhatt MJ, Farabaugh PJ. Codon-specific effects of tRNA anticodon loop modifications on translational misreading errors in the yeast *Saccharomyces cerevisiae*. Nucleic Acids Res. 2018;46:10331–10339.
4. Benítez-Páez A, Villarroya M, Armengod ME. The *Escherichia coli* RlmN methyltransferase is a dual-specificity enzyme that modifies both rRNA and tRNA and controls translational accuracy. RNA. 2012;18:1783–1795.
5. Yarian C, Townsend H, Czestkowski W, et al. Accurate translation of the genetic code depends on tRNA modified nucleosides. J Biol Chem. 2002;277, 16391–16395.
6. Maehigashi T, Dunkle JA, Miles SJ, Dunham CM. Structural insights into +1 frameshifting promoted by expanded or modification-deficient anticodon stem loops. Proc Natl Acad Sci U S A. 2014;111:12740–12745.
7. Nguyen HA, Hoffer ED, Dunham CM. Importance of a tRNA anticodon loop modification and a conserved, noncanonical anticodon stem pairing in tRNACGGPro for decoding. J Biol Chem. 2019;294:5281–5291.
8. Urbonavičius J, Qian Q, Durand JMB, Hagervall TG, Björk GR. Improvement of reading frame maintenance is a common function for several tRNA modifications. EMBO J. 2001;20:4863–4873.
9. Ranjan N, Rodnina MV. Thio-modification of tRNA at the wobble position as regulator of the kinetics of decoding and translocation on the ribosome. J Am Chem Soc. 2017;139, 5857–5864.
10. Phelps SS, Malkiewicz A, Agris PF, Joseph S. Modified nucleotides in tRNALys and tRNAVal are important for translocation. J Mol Biol. 2004;338(3), 439–444.
11. Salman Ashraf S, Sochacka E, Cain R, Guenther R, Malkiewicz A, Agris PF. Single atom modification (O → S) of tRNA confers ribosome binding. RNA. 1999;5:5–194.
12. Weixlbaumer A, Murphy FV, Dziergowska A, et al. Mechanism for expanding the decoding capacity of transfer RNAs by modification of uridines. Nat Struct Mol Biol. 2007;14, 498–502.
13. Madore E, Florentz C, Giegé R, Sekine SI, Yokoyama S, Lapointe J. Effect of modified nucleotides on Escherichia coli tRNA(Glu) structure and on its aminoacylation by glutamyl-tRNA synthetase. Predominant and distinct roles of the mnm5 and s2 modifications of U34. Eur J Biochem. 1999;266:1128–1135.

14. Clifton BE, Fariz MA, Uechi G-I, Laurino P. Evolutionary repair reveals an unexpected role of the tRNA modification m1G37 in aminoacylation. Nucleic Acids Res. 2021;49:12467–12485.
15. Begley U, Dyavaiah M, Patil A, et al. Trm9-catalyzed tRNA modifications link translation to the DNA damage response. Mol Cell. 2007;28:860–870.
16. Lin H, Miyauchi K, Harada T, et al. CO2-sensitive tRNA modification associated with human mitochondrial disease. Nat Commun. 2018;9:1875.
17. Esberg B, Bjork GR. The methylthio group (ms2) of N6-(4-hydroxyisopentenyl)-2- methylthioadenosine (ms2io6A) present next to the anticodon contributes to the decoding efficiency of the tRNA. J Bacteriol. 1995;177:1967–1975.
18. Zhou H, Kimsey IJ, Nikolova EN, et al. M1A and m1G disrupt a-RNA structure through the intrinsic instability of Hoogsteen base pairs. Nat Struct Mol Biol. 2016;23:803–810.
19. Denmon AP, Wang J, Nikonowicz EP. Conformation effects of base modification on the anticodon stem–loop of Bacillus subtilis tRNATyr. J Mol Biol. 2011;412:285–303.
20. Cabello-Villegas J, Tworowska I, Nikonowicz EP. Metal ion stabilization of the U-turn of the A 37 N 6-dimethylallyl-modified anticodon stem-loop of *Escherichia coli* tRNA Phe. Biochemistry. 2004;43(1):55–66.
21. Cabello-Villegas J, Winkler ME, Nikonowicz EP. Solution conformations of unmodified and A37N6-dimethylallyl modified anticodon stem-loops of Escherichia coli tRNAPhe. J Mol Biol. 2002;319:1015–1034.
22. Murphy FV, Ramakrishnan V, Malkiewicz A, Agris PF. The role of modifications in codon discrimination by tRNA Lys UUU. Nat Struct Mol Biol [Internet]. 2004;11:1186–1191.
23. Sundaram M, Durant PC, Davis DR. Hypermodified nucleosides in the anticodon of tRNA Lys stabilize a canonical U-turn structure †, ‡. Biochem Int. 2000;39:12575–12584.
24. Golovina AY, Sergiev PV, Golovin AV, et al. The yfiC gene of E. coli encodes an adenine-N6 methyltransferase that specifically modifies A37 of tRNA1Val(cmo5UAC). RNA. 2009;15:1134–1141.
25. Andachi Y, Yamao F, Muto A, Osawa S. Codon recognition patterns as deduced from sequences of the complete set of transfer RNA species in mycoplasma capricolum resemblance to mitochondria. J Mol Biol. 1989;209:37–54.
26. De Crécy-Lagard V, Marck C, Brochier-Armanet C, Grosjean H. Comparative RNomics and Modomics in mollicutes: Prediction of gene function and evolutionary implications. IUBMB Life. 2007;59:634–658.
27. Schubert HL, Blumenthal RM, Cheng X. Many paths to methyltransfer: A chronicle of convergence. Trends Biochem Sci. 2003;28:329–335.
28. Holm L. Using Dali for protein structure comparison. Methods in molecular biology. Volume 2112, 2020; p. 29–42. New York, NY: Humana.
29. Krissinel E, Henrick K. Inference of macromolecular assemblies from crystalline state. J Mol Biol. 2007;372:774–797.
30. Wang X, Feng J, Xue Y, et al. Structural basis of N6-adenosine methylation by the METTL3-METTL14 complex. Nature. 2016;534:575–578.
31. Wang P, Doxtader KA, Nam Y. Structural basis for cooperative function of Mettl3 and Mettl14 methyltransferases. Mol Cell. 2016;63:306–317.
32. Doxtader KA, Wang P, Scarborough AM, Seo D, Conrad NK, Nam Y. Structural basis for regulation of METTL16, an S-sdenosylmethionine homeostasis factor. Mol Cell [internet]. 2018;71:1001–1011.e4. https://doi.org/10.1016/j.molcel.2018.07.025.
33. Ren W, Lu J, Huang M, et al. Structure and regulation of ZCCHC4 in m6A-methylation of 28S rRNA. Nat Commun. 2019;10:5042.
34. Ruszkowska A, Ruszkowski M, Dauter Z, Brown JA. Structural insights into the RNA methyltransferase domain of METTL16. Sci Rep. 2018;8:1–13.
35. Punekar AS, Liljeruhm J, Shepherd TR, Forster AC, Selmer M. Structural and functional insights into the molecular mechanism of rRNA m6A methyltransferase RlmJ. Nucleic Acids Res. 2013;41:9537–9548.
36. Van Tran N, Ernst FGM, Hawley BR, et al. The human 18S rRNA m6A methyltransferase METTL5 is stabilized by TRMT112. Nucleic Acids Res. 2019;47:7719–7733.
37. Kettani A, Guéron M, Leroy JL. Amino proton exchange processes in mononucleosides. J Am Chem Soc. 1997;119:1108–1115.
38. Sakaguchi R, Lahoud G, Christian T, Gamper H, Hou YM. A divalent metal ion-dependent N1-methyl transfer to G37-tRNA. Chem Biol. 2014;21:1351–1360.
39. Perlinska AP, Kalek M, Christian T, Hou YM, Sulkowska JI. Mg2+-dependent methyl transfer by a knotted protein: A molecular dynamics simulation and quantum mechanics study. ACS Catal. 2020;10:8058–8068.
40. Hyeonju Jeong JK. Unique anticodon loop conformation with the flipped-out wobble nucleotide in the crystal structure of unbound tRNAVal. RNA. 2021;27:1330–1338.
41. Yan Y, Zhang D, Zhou P, Li B, Huang SY. HDOCK: A web server for protein-protein and protein-DNA/RNA docking based on a hybrid strategy. Nucleic Acids Res. 2017;45:W365–W373.
42. Losey HC, Ruthenburg AJ, Verdine GL. Crystal structure of *Staphylococcus aureus* tRNA adenosine deaminase TadA in complex with RNA. Nat Struct Mol Biol. 2006;13:153–159.
43. Byrne RT, Jenkins HT, Peters DT, et al. Major reorientation of tRNA substrates defines specificity of dihydrouridine synthases. Proc Natl Acad Sci U S A. 2015;112:6033–6037.
44. Hoang C, Chen J, Vizthum CA, et al. Crystal structure of pseudouridine synthase RluA: Indirect sequence readout through protein-induced RNA structure. Mol Cell. 2006;24:535–545.
45. Xie W, Liu X, Huang RH. Chemical trapping and crystal structure of a catalytic tRNA guanine transglycosylase covalent intermediate. Nat Struct Biol. 2003;10:781–788.

SUPPORTING INFORMATION

Additional supporting information may be found in the online version of the article at the publisher's website.

How to cite this article: Jeong H, Lee Y, Kim J. Structural and functional characterization of TrmM in m^6A modification of bacterial tRNA. Protein Science. 2022;31(5):e4319. https://doi.org/10.1002/pro.4319